Separation and Purification Technology 354 (2025) 129314

Contents lists available at ScienceDirect

Separation and Purification Technology

journal homepage: www.elsevier.com/locate/seppur

Polyelectrolyte-coated zeolite-templated carbon electrodes for capacitive deionization and energy generation by salinity exchange

Sergio Orozco-Barrera [a], Keigo Wakabayashi [b], Takeharu Yoshii [b], Hirotomo Nishihara [b,c], Guillermo R. Iglesias [a,d], Ángel V. Delgado [a,d], Silvia Ahualli [a,*]

[a] Department of Applied Physics, University of Granada, Granada, Spain
[b] Institute of Multidisciplinary Research for Adv Mater (IMRAM), Tohoku University, Sendai, Japan
[c] Advanced Institute for Materials Research (WPI-AIMR), Tohoku University, Sendai, Japan
[d] Instituto de Investigación Biosanitaria ibs.GRANADA, NanoMag Laboratory, Granada, Spain

ARTICLE INFO

Editor: Luo Guangsheng

Keywords:
Zeolite-templated carbon
Capacitive deionization
Capacitive mixing
Polyelectrolytes
Ion-exchange membranes
Electrokinetics

ABSTRACT

As global demands for freshwater and renewable energy intensify, capacitive deionization (CDI) emerges as a promising technique for water purification, desalination, and ionic separation. Reciprocally, energy harvesting has been made possible from exchanging solutions with different salinity, using the so-called capacitive mixing (CapMix) methods, now taking their first steps towards a wider range of application. In all the techniques mentioned, porous electrodes are used in order to maximize the stored charge, making it essential to properly select the material of which the electrode is composed. This work focuses on exploring the performance of zeolite-templated carbon (ZTC) as a highly promising electrode material. ZTC offers ordered pore distribution and high electrical conductivity, making it in principle ideal for energy harvesting and water purification applications. In order to optimize its performance, the surface of the ZTC is for the first time modified by application of polyelectrolyte coatings, resulting in so-called soft electrodes or SEs. This combination of electrode material and functionalization gives rise to a highly efficient and low energy-consuming strategy to fully realize the potential of this carbon material in CDI and CapMix techniques for tackling global freshwater and energy challenges. Energy and power generation values up to 25 mJ and 7.5 mW m^{-2} have been obtained (with measured potential rises of 131 mV by only exchanging salinities of the bathing solution), which overcome values such as 4.3 mW m^{-2} previously found in our laboratory under similar conditions.

1. Introduction

The increasing demand for fresh water has made imperative to explore innovative technologies that can provide clean water in a sustainable and renewable way, using the required energy in a cost-effective and efficient way. As an example, capacitive deionization (CDI) is a promising technology that has emerged as potential solution to desalinate brackish water. The process is based on the electric double layer (EDL) properties [1,2]. When the solid surface acquires charge (because of the applied potential, in the case of electrodes) ions charged opposite to the surface (counterions) are attracted to it, and form the diffuse charged layer accumulating in that region until the electrode surface charge gets screened. As a result, ions of both signs are removed from the solution by electrostatic attraction to the corresponding opposite electrode. The repulsion (desorption) of coions (with the same charge sign as the respective electrode) is smaller than counterion adsorption as long as the surface charge is high enough, with the net result of partial desalination. The EDL has properties typical of a capacitor, with large capacitance if porous electrodes with high surface area are used [3,4]. Roughly speaking, the plate distance of that capacitor is smaller if the solution in contact has a high ionic strength (compressed EDL) than when it is bathed by a low ionic strength solution

Abbreviations: AC, Activated Carbon; CapMix, Capacitive Mixing; CB, Carbon Black; CDI, Capacitive Deionization; CDLE, Capacitive Energy Extraction based on Double Layer Expansion; CDP, Capacitive Energy Extraction based on Donnan Potential; EDL, Electric Double Layer; IEMs, Ion Exchange Membranes; OCV, Open Circuit Voltage; PDADMAC, Poly(diallyldimethylammonium chloride); PSS, Poly(sodium 4-styrenesulfonate); PVDF, Poly(vinylidene fluoride); SAC, Specific Adsorption Coefficient; SEs, Soft Electrodes; TEM, Transmission Electron Microscopy; ZTC, Zeolite-templated carbon.

* Corresponding author at: Departamento de Física Aplicada, Facultad de Ciencias, Universidad de Granada, 18071 Granada, Spain.
E-mail address: sahualli@ugr.es (S. Ahualli).

https://doi.org/10.1016/j.seppur.2024.129314
Received 27 May 2024; Received in revised form 10 August 2024; Accepted 20 August 2024
Available online 30 August 2024

(expanded EDL).

The latter property is basic to the harvesting of energy by salinity gradient employing the so-called CapMix methods [5–9]. These are based on charging a pair of electrodes while in contact with a salty solution (high capacitance) and discharging them after exchanging (at constant charge) the in-contact solution with fresh water (low capacitance). In the process, a rise in the potential difference between the electrodes takes place, so that more energy is received than it was used in charging. This means that the method has the potential to provide a renewable and sustainable source of energy arising from salinity gradients.

The choice of materials is essential for the efficiency and effectiveness of both CDI and CapMix techniques, as their electrical conductivity and available surface area play a crucial role in the performance of the electrodes. Activated carbon (AC) and other carbon-based materials are often used as an electrode composite for CDI and energy harvesting [10–17] due to their high surface area and pore size distribution, which have been shown to enhance the efficiency of these processes significantly. However, we have found[1] that the tortuosity of the macropores hinders the diffusive processes in their interior, causing a slow response and an incomplete use of the nominally available area.

Zeolite-templated carbon (ZTC) is a promising material that has awakened great interest in its use for capacitive electrodes as it possesses a unique combination of the above-mentioned characteristics [18–20]. ZTC is formed over zeolite templates which are later removed, leaving behind a carbon matrix with a well-defined pore structure [19,21,22] consisting of single-layer curved graphene frameworks. The resulting material has a high surface area and excellent electrical conductivity, making it an ideal electrode material for CDI and CapMix applications. Moreover, the pore size of ZTC can be adapted to the base framework used for its formation, potentially allowing improved performance in terms of ion removal as it possesses large easy-diffusion paths for ionic transport [23].

Both CDI and CapMix techniques have been shown to improve if ion-exchange membranes (IEMs) are used in conjunction with carbon electrodes. Within the realm of membrane-assisted CDI, IEMs play a pivotal role in significantly enhancing the efficiency of ion removal. This is achieved through blocking the transport of co-ions from the electrode pores to the solution while facilitating the transport of counter-ions to the electrodes [24–28]. Concerning the CapMix processes, IEMs come into play by creating a natural potential difference between electrodes through Donnan equilibrium, thus obviating the requirement for an external power source. This approach is denoted as capacitive energy extraction based on Donnan potential (CDP) [29,30].

An alternative approach, based on coating the carbon with charged polymer layers (polyelectrolyte coating or soft-electrode −SE- configuration) is the target in the present work, as a compelling, membrane-free approximation to the increase in both CDI [31–33] and CDP [6,34] performances. As additional advantages, the coatings provide longer electrode lifetime and enhancing of their wettability. Importantly, SEs also yield economic advantages and facilitate the preparation process in comparison to attached IEMs. Furthermore, a synergistic approach was explored through the combination of polyelectrolyte coatings with IEMs. SEs are established as a suitable support for IEMs, resulting in a substantial improvement of the overall system performance [35,36].

To our knowledge, the zeolite-templated carbons have been previously studied for their use as gas adsorbents, in supercapacitors, batteries and catalysis [37–41], but little work has been dedicated to their use in capacitive deionization [42] or, to an even lesser extent, in CapMix applications. Moreover, the addition of polyelectrolyte-coatings to ZTC has not been explored to date. In this work, we investigate the combination of zeolite-templated carbon electrodes with polyelectrolyte and IEMs coatings for CapMix, CDI and CDP techniques. The aim is taking full advantage of the ordered surface properties of the carbon material associated to the advantage of the polymer coatings. The potential benefits of these technologies for sustainable, renewable resource management make them part of important, near-future research focus.

2. Capacitive deionization

In CDI or CDP the desalination process takes place by continuously pumping a saline solution through the measurement cell. Each CDI cycle consists of two stages: during adsorption, a constant voltage or current is applied to the cell, driving ions from the bulk solution to the micropores of their counter-electrode. Desorption is carried out once the surface charge of the electrodes get neutralized by the counterions; this stage is required in order to drain the pores to be ready for their use in consecutive cycles. Desorption occurs when applying an opposite potential difference to the cell (Reverse-Voltage method) thus forcing the ions to exit the pores. In the present work, the used saline solution was 10 mM KCl, chosen for this study as a model solution due to the similarities between K^+ and Cl^- diffusion coefficients in water (1.96×10^{-9} $m^2\ s^{-1}$ and 2.03×10^{-9} $m^2\ s^{-1}$, respectively, at 25 °C).

The performance of each electrode configuration is usually quantified via the salt adsorption capacity (*SAC*) and the charge efficiency of the process [10,43]. *SAC* expresses the ratio between the mass of adsorbed ions and that of solid carbon electrode (including the binder mass as part of the total mass of the electrode), and is proportional to the area enclosed by the concentration difference curve in the adsorption stage:

$$SAC = \frac{M_{salt}}{m_{elect}} n \tag{1}$$

M_{salt} is the molar mass of the saline component, m_{elect} is the total electrode mass, and n is the number of adsorbed moles, which can be calculated as [43,44]:

$$n = \int_0^{t_{ads}} (c_{out}(t) - c_{in})\, \varphi_v \; dt \tag{2}$$

Being $c_{out}(t)$ the instantaneous measured concentration at the cell outlet, c_{in} the feed solution concentration, φ_v the pumping flow rate of the solution through the cell; the integration goes from $t = 0$ to $t = t_{ads}$, duration time of an adsorption stage.

The ratio between the total amount of salt adsorbed and the charge transferred between the electrodes in the adsorption stage time provides the charge efficiency of the system, Δ[45]. It will reach its maximum value (equal to 1) when an ion is retired per unit charge deposited on the electrodes [46]:

$$\Delta = F\frac{\int_0^{t_{ads}} (c_{out}(t) - c_{in})\, \varphi_v \; dt}{Q} = F\frac{\int_0^{t_{ads}} (c_{out}(t) - c_{in})\, \varphi_v \; dt}{\int_0^{t_{ads}} I(t)\, dt} \tag{3}$$

where Q is the stored charge during the adsorption stage, $I(t)$ is the instantaneous current, and F is the Faraday constant.

3. Capacitive mixing (CapMix)

The setup used for Capacitive Energy Extraction based on Donnan Potential (CDP) measurements is arranged on the same cell used for CDI, in which ion exchange membranes and SEs are used to establish a spontaneous electric potential difference between the electrodes. Salty and fresh solutions are alternatively pumped when necessary. CDP in CapMix is based on the following steps [47], which are graphically shown in Fig. 1.a:

A. Initially, uncharged functionalized electrodes are bathed in salty water, establishing Donnan potentials. As the electrodes are not charged, there is no EDL potential, and the surface potential of each electrode matches the Donnan potential. For symmetrical electrodes, the potential difference between them will be twice the Donnan potential.

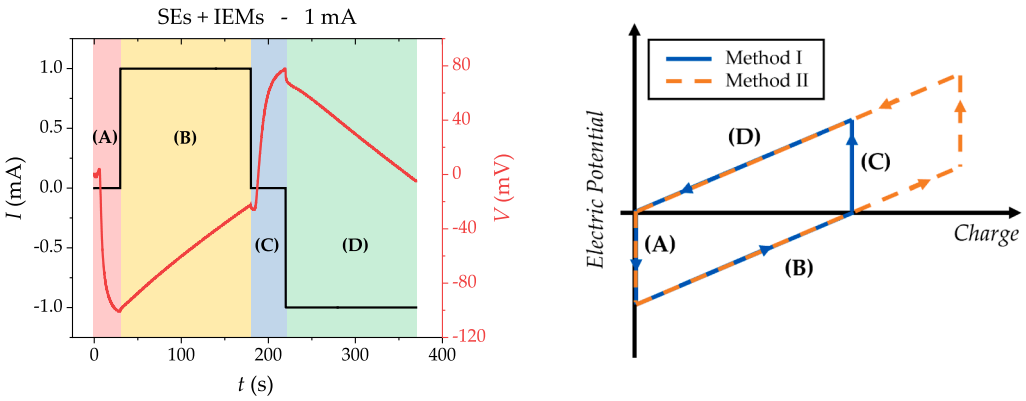

Fig. 1. Applied current (black) and measured electric potential (red) as a function of time for a whole CDP cycle, used as a visual example of the direct measurements for each stage of the method. For this example, the cycle corresponding to SEs + IEMs has been used. Regions (A) and (C) correspond to fresh-to-salty and salty-to-fresh solutions being interchanged in open circuit, respectively. In regions (B) and (D), constant current values are applied, corresponding to positive and negative charge transfer steps with salty and fresh solutions as electrolyte, respectively. Right: Schematic electric potential vs. stored charge for Method I and Method II (see text). Cycle stages are also marked in this scheme. (For interpretation of the references to colour in this figure legend, the reader is referred to the web version of this article.)

B. Both electrodes are connected externally to transfer charge from one to the other (positive charge transfer), forming EDLs near the surfaces. The EDL potential counterbalances the Donnan potential, and both electrodes become equipotential, causing charge transfer to stop. This step can be controlled by applying a constant current through an external source. This is not essential, but practically useful.
C. Fresh water is pumped in, and the external circuit is disconnected, resulting in an increase in the absolute value of both Donnan and EDL potentials due to the lower concentration of the bathing solution and the expansion of the double layer at fixed surface charge. The Donnan potential increase is larger, resulting in a net increase in both surface potentials.
D. The electrodes are reconnected (as before, with or without a constant current source), leading to a negative charge flow until equipotentiality is restored, and the potential at the surface returns to zero due to the system's symmetry.
E. Finally, the circuit is reopened, and the fresh water is replaced with salty water. This step is equivalent to step A, and re-closing the circuit and applying positive charge transfer brings the process forward to step B.

As mentioned above, the performance of CDP measurements can be quantified via the obtained energy in the cycles, E, and the power per unit projected area of electrodes, P, of the process [47]. The energy obtained in each of the cycles is equal to the area enclosed by the electric potential vs. stored charge curve. The charge is calculated by integrating the instantaneous electric current, $I(t)$, through the cycle, and so E can be calculated as:

$$E = \int_0^{t_{cycle}} V(t)\, I(t)\, dt \tag{4}$$

The power per unit area is calculated as:

$$P = \frac{E}{S_{elect}\, t_{cycle}} \tag{5}$$

Being S_{elect} the projected area of the electrodes, and t_{cycle}, the duration time of the cycle.

4. Experimental

4.1. Materials

For the experimental work, 10 mM, 20 mM and 500 mM KCl solutions (Merck-Sigma Aldrich, Germany) were prepared and used as electrolytes. Water was deionized and filtered using a Milli-Q Academic System (Millipore, France). Zeolite-templated carbon (ZTC) particles [18–22] were used as main material for the preparation of the electrodes (Fig. 2a). The pore size distribution averages to ~ 1.2 nm, and its surface area is equal to 4005 m^2/g. Carbon Black (Alfa Aesar, Thermo Fisher, Germany), with a surface area of 57–67 m^2/g, has also been used as a minor additive for improving overall electric conductivity [48]. Poly (diallyldimethyl-ammonium chloride) (PDADMAC, with a molecular weight of 200,000 g/mol) and poly(sodium 4-styrenesulfonate) (PSS, with a molecular weight of 100,000 g/mol) were used as, respectively, cationic and anionic polyelectrolytes for coating the electrodes (both polymers were purchased from Sigma-Aldrich, Darmstadt, Germany). The IEMs used were AMX and CMX (Neosepta, Tokuyama, Japan) as anion and cation exchange membranes, respectively, with corresponding thicknesses of 140 μm and 170 μm.

4.2. Methods

4.2.1. Electrode setup

The experimental setup is based on two planar electrodes, facing each other, and separated 500 μm by a rubber spacer (see Fig. 2b). Each of these electrodes was formed by a 5 cm wide and 10 cm long graphite plate used as a current collector, onto which the carbon was deposited. Carbon particles suspensions were prepared by mixing zeolite-templated carbon (ZTC), Carbon Black (CB) (95:5) and a 33 g/L solution of poly (vinylidene-fluoride) (PVDF, manufactured by Arkema, Colombes, France, as Kynar HSV 900, with molecular weight approximately 1,000,000) in 1-methyl 2-pyrrolidone (Sigma Aldrich, Darmstadt, Germany). The product was formed by mixing 3 g of the ZTC+CB mixture with 10 g of the PVDF solution until a slurry was formed. The final carbon suspension was deposited onto the graphite collectors as a layer and dried at 70 °C overnight. For the membranes assembly to the electrodes, the anion (cation) exchange membrane was placed next to the electrode which works as cathode (anode).

For SEs preparation, the polymeric coating was made by immersing (for 24 h under constant magnetic stirring) the carbon powder in a 200 mM (on a monomer basis) aqueous solution of the corresponding polyelectrolyte. The resulting suspension was centrifuged and

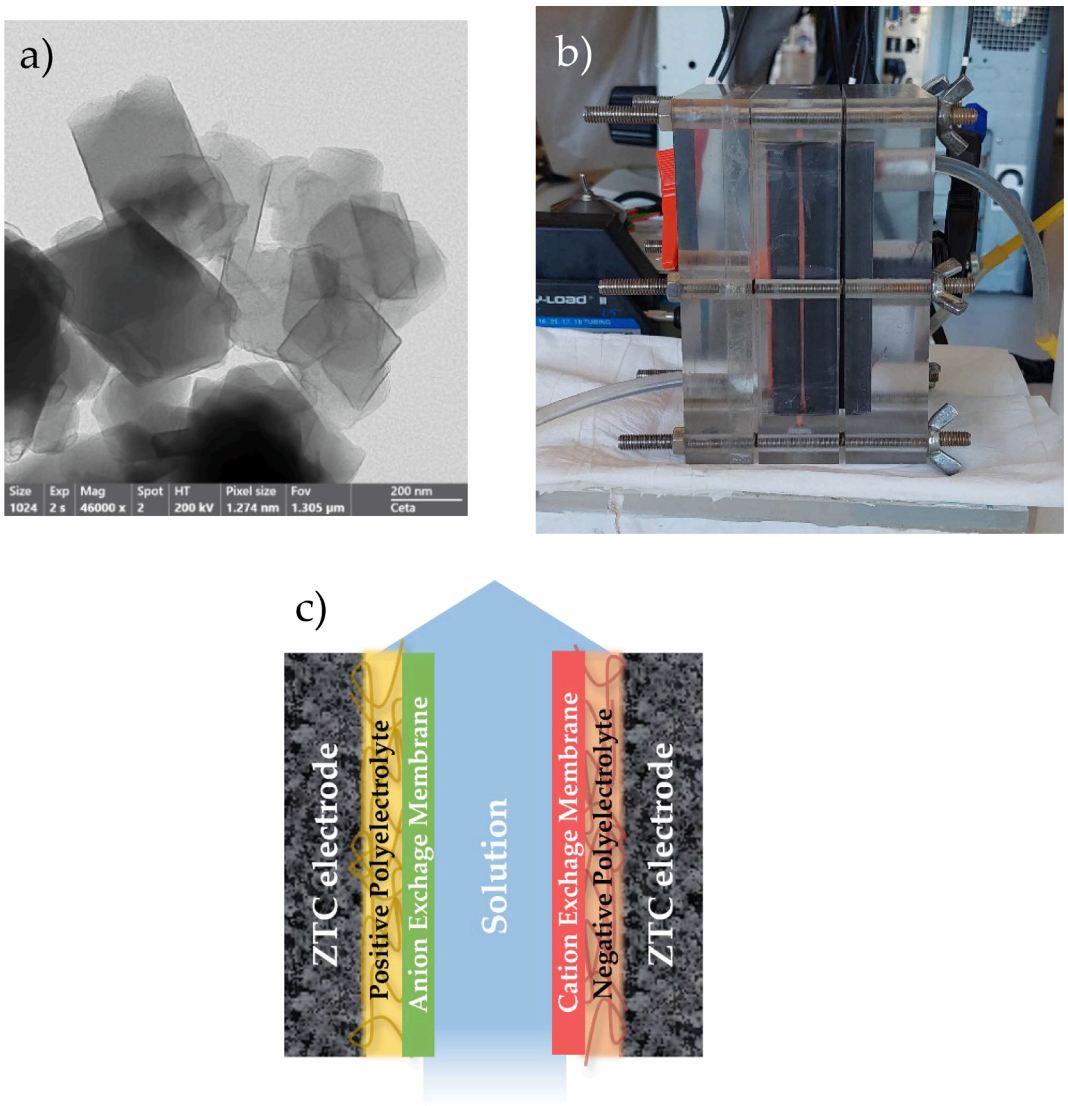

Fig. 2. a) Transmission electron microscopy (TEM) image of the ZTC particles. Scale bar is 200 nm. b) Photograph of the measurement cell. Two graphite plates are used as current collectors and support for the carbon electrodes, which are separated by a rubber ring. Cell inlet and outlet for the solutions are also shown at the lower-left corner and the upper-right one, respectively. c) Cell scheme with functionalized ZTC electrodes covered with ion exchange membranes.

redispersed in water, and this cleaning process was repeated thrice. Polymer-coated carbon was then set to dry overnight at 50 °C. Once the coating was finished, SEs were prepared by mixing polyelectrolyte-coated carbon powders with PVDF as binder following the steps described above, being one of the electrodes cationic and the other anionic. As depicted in Fig. 2c, a soft-electrode/membrane combination can be used by placing the cation(anion)-exchange membrane onto the negatively(positively) functionalized ZTC.

4.2.2. Particles structural characterization

Powder X-ray diffraction patterns were obtained using a Rigaku MiniFlex600 (Japan) (Cu-Kα radiation, 40 kV, 15 mA, 1.5418 Å) between 2 and 50° (2θ) with a 0.02° step. N_2 adsorption isotherms were obtained using a MicrotracBEL Corp. (Japan), BELSORP-max system at −196 °C. The Brunauer-Emmett-Teller (BET) surface area (S_{BET}) was calculated using the multipoint BET method from the adsorption data in the range of $P/P_0 = 0.01–0.05$ [49]. The total pore volume (V_{total}) was calculated from the adsorption amount at $P/P_0 = 0.96$. The pore-size distribution was calculated with the non-local density functional theory (NLDFT) using a slit-pore model [50].

4.2.3. Particles electrical characterization

Electrophoretic mobilities of the carbon powders, both bare and polyelectrolyte-coated, were measured to check if the coatings were carried out successfully. Determinations were performed at pH 6 in 1 mM KCl solutions, in a Malvern Zetasizer NanoZS (Malvern Panalytical, UK). An almost neutral value for the bare ZTC mobility was obtained $(0.4 \pm 0.5) \times 10^{-8}\ m^2\ V^{-1}s^{-1}$ (or a zeta potential estimation of 5.1 ± 6.4 mV, based on the Helmholtz-Smoluchowski equation), i.e., almost zero, as expected from the high electrical conductivity of this material. On the other hand, both PDADMAC-coated and PSS-coated carbons show a clearly positive and negative electrophoretic mobility, with values of $(3.71 \pm 0.01) \times 10^{-8}\ m^2\ V^{-1}\ s^{-1}$ (47.49 ± 0.13 mV) and $(-3.16 \pm 0.06) \times 10^{-8}\ m^2\ V^{-1}\ s^{-1}$ (−40.45 ± 0.77 mV), respectively.

4.2.4. CDI method

The cell was connected to an IviumStat.h Potentiostat (Ivium Technologies, The Netherlands), by means of which we were able to control and measure the voltage and current applied to the system. Changes in conductivity (and temperature) were measured at the exit of the cell with a 529.670 conductivity/temperature probe (Leybold, Germany) and continuously recorded by a Leybold 524D10 Cassy Lab interface.

The exit solution was returned to the original vessel (large enough to keep constant inlet conductivity values during successive working cycles).

4.2.5. Energy harvesting methodology

The cell setup was also connected to the potentiostat in order to apply current and measure potential difference between electrodes in the different cycle stages (Fig. 1). The digital outputs of this device allow also the control of the pumps feeding the low- and high-salt solutions and the setting of open circuit when solutions are exchanged. Two variations of the CDP experimental method have been followed in this work, where the cycles have been forced to reach specific total stored charges instead of applying a neutral potential condition for the charge transfer to stop (see Fig. 1.b):

I. In Method I, equal time values were set for both positive and negative charge transfer stages in order to achieve almost equipotential values after the charge has been transferred, similar to a "self-generated" process. The establishment of these preset times for constant current application forces the stored charge to remain the same during consecutive cycles, which reduces the natural residual charge leakages of the cell. Optimum experimental parameter values were found by applying currents of ± 1 and ± 2 mA for positive and negative charge transfer, with different times depending on the studied cell configuration. Furthermore, in order to optimize both energy and power obtained from the cycles, preset time values were also chosen for open cell stages, where the salinity of the electrolyte was being interchanged and thus the electric potential experienced an increase or a decrease. These stages lasted until the voltage variation reaches its maximum absolute value.
II. In Method II, currents of ± 1 mA were set for positive and negative charge transfer steps, respectively, but their application times were doubled with respect to Method I, forcing the cycles to explore wider charge windows (horizontal expansion) with the aim of maximizing the obtained energy [29,47].

5. Results and discussion

5.1. Structural characterization

The x-ray diffractogram of bare ZTC is plotted in Fig. 3. Note the presence of maxima corresponding to (111) and (220) reflections, characteristic of ZTC [22].

The BET analysis of nitrogen adsorption–desorption experiments is described in Fig. 4. As observed, a well-defined pore diameter distribution is obtained, with a range of diameters between 1 and 2 nm. The surface area of the bare sample amounts to 4005 m^2/g, well in the range reported previously for ZTC [18] and much higher than values typical for activated carbon (on the order of 2000 m^2/g [14]). Finally, infrared spectra have already been reported in Ref. 51.

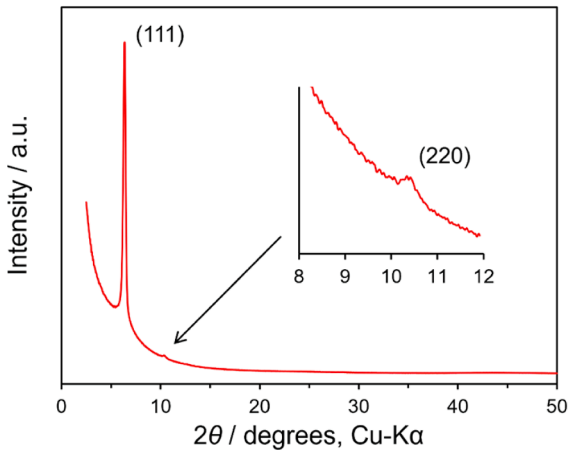

Fig. 3. X-ray diffraction data obtained for the bare ztc powder.

5.2. Capacitive deionization (CDI) performance

The behavior and performance of CDI cycles are based on the ion adsorption occurring during the process. Ion removal from the bulk solution translates into a conductivity drop until the charge of the electrodes is screened by the EDL, and then it returns to the feed solution value after reaching a minimum, as the solution is constantly pumped. Ion adsorption is proportional to the area enclosed by the concentration difference curve in the adsorption stage, being greater the number of ions removed the larger is the area under the curve.

CDI measurements were performed for bare carbon electrodes, polyelectrolyte-coated ones, electrodes with IEM and the combination of the last two coatings (Fig. 5.a). A 10 mM KCl solution was used as electrolyte for these measurements and constant voltages of 0.9 V were used for the adsorption stage with 300 s of duration. The measured curves show a huge improvement in the concentration changes during adsorption by functionalizing the ZTC electrodes or supporting them with IEMs. The curves in which the use of membranes is involved seem to reach the maximum concentration differences at shorter times; however, when SEs are involved, ion adsorption extends during longer times. Combining SEs with membranes gives way to a mixed behavior by presenting a concentration difference peak as high as that obtained with membranes, while keeping an SE-characteristic long-lasting adsorption.

Quantitative values of salt adsorption capacity, *SAC*, as a function of time are shown in Fig. 5.b. In all cases this coefficient is cumulative, increasing with time, until it adopts a linear trend that coincides with a constant concentration difference. This indicates that there is no more adsorption on the electrodes and, therefore, determines the time limit that will be used to calculate the cumulative salt adsorption using Eq. (2) (t_{ads}). In Fig. 5.b, the straight lines accompanying the *SAC* curves are a guide to determine the linear behaviour serving as an indicator of the cutoff time for each electrode configuration (i.e., the time beyond which the linear trend is established). Final *SAC* values and charge efficiency are shown in Table 1.

It is remarkable that both SEs and SEs + IEMs give way to better performances, reaching the highest SAC values (10.9 ± 0.1 mg/g and 11.1 ± 0.1 mg/g, respectively) and high efficiencies up to 0.90, overcoming the performance of stand-alone membranes. The energetic cost per ion removed can also be calculated as the ratio between the total number of adsorbed moles and the charge transferred between the electrodes in the adsorption time, providing a very favorable value of (20.0 ± 0.1) k_BT compared to previously obtained results in our laboratory [52] and also reported by other authors [53,54], remaining between $30k_BT - 80k_BT$ for CDI and $15k_BT - 40k_BT$ for MCDI [43]. Also, the combined use of IEMs and SEs does not seem to offer remarkable quantitative differences. To explain that we can recall that the role of each of these coatings is the blocking of coion migration from the electrode pores to the bulk solution, and such effect improves the efficiency. In this way, if one of the coatings (either polyelectrolyte or membrane) plays this role optimizing performance almost to the maximum, the superposition of a second coating will not affect the result, maintaining values close to 1 for efficiency and barely influencing the SAC.

It should be noted that the SAC values obtained in this work are based on the application of a 0.9 V potential difference between the electrodes. The use of higher voltages, up to 1.2 V or 1.4 V, results in much larger SAC values for SEs + IEMs, reaching (17.6 ± 0.1) mg/g and (30.5 ± 0.1) mg/g, respectively, with efficiencies as high as 0.9 (see Figure S1 and Table S1). These values are comparable with some of the highest SAC values obtained for porous hollow carbon nanoboxes (HCNBs) according the results published very recently [42].

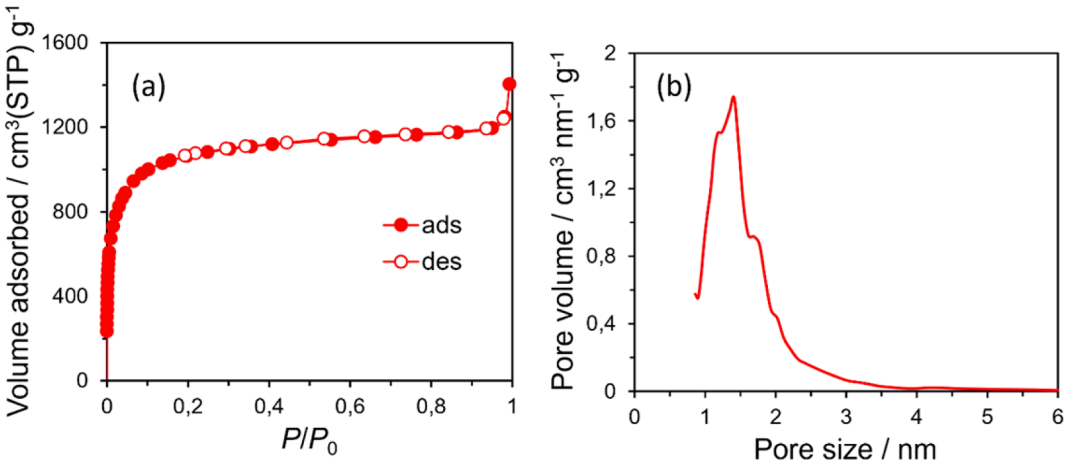

Fig. 4. (a) N_2 adsorption–desorption data for bare ZTC. (b) Pore volume distribution obtained from (a).

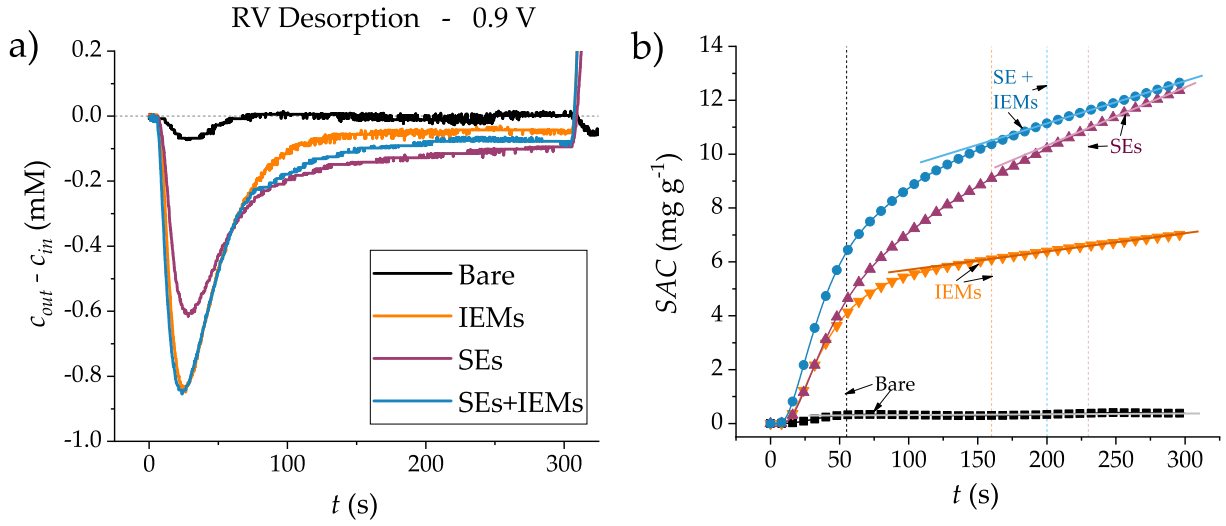

Fig. 5. Concentration differences measured at the cell outlet (a), and Specific Adsorption Capacity, *SAC* (b) as a function of time in the adsorption stage for each electrode configuration (bare carbon; covered with ion-exchange membranes (IEMs); coated with polyelectrolytes (SEs); assembly of polyelectrolyte-coated and ion exchange membranes (SEs + IEMs)). The applied voltage was 0.9 V and a 10 mM KCl solution was used as electrolyte. In b), the dashed vertical lines indicate where the time limit for the SAC calculation is set in each case, corresponding to the onset of the linear trends indicated by the solid lines.

Table 1
SAC and charge efficiency values calculated for each electrode configuration.

Electrode configuration	*SAC* (mg g^{-1})	Charge efficiency
Bare	0.3 ± 0.2	0.03 ± 0.05
SEs	10.9 ± 0.1	0.90 ± 0.02
IEMs	6.1 ± 0.1	0.76 ± 0.03
SE+IEMs	11.1 ± 0.1	0.88 ± 0.02

The combination of SEs + IEMs has also been explored in a previous work for high-salinity water desalination although using other carbon material. SAC values of less than 8 mg/g and efficiencies rounding 0.60 were reported when the solution to desalinate was 100 mM NaCl [35]. The use of ZTC in the same procedure leads to a SAC value of (25.3 ± 0.1) mg/g with efficiency up to 0.84 (see Figure S2 and Table S2), bringing some light to the use of CDI with carbons having pores which are not sub-nanometer in size, and presenting ordered pore-structure for these purposes [43,54–56].

Note that the CDI performance of bare particles is small because of the reverse voltage method used in the discharge step; this method produces adsorption and desorption ("frequency doubling") at the same time, as it has been also found for other carbon materials [35]. In contrast, a substantial improvement is observed in *SAC* and efficiency when the carbon is functionalized by polyelectrolyte coatings and when IEMs are placed onto the electrodes while working under reverse voltage method. After these treatments, the SAC values found in this investigation are almost twice larger than reported for other previously studied carbon materials with the same coatings [35]. More important, the charge efficiency reaches almost unity (to be compared to approximately 0.7 in the best configuration described in Ref. [35]), indicating that the structure pattern of the ZTC particles allows a very efficient coating.

The functionalization, in addition, improves the hydrophilicity of the ZTC; to confirm this assumption, contact angle measurements were carried out, based on images of water droplets on the surface of bare and soft electrodes. Droplet photographs were taken using a PixeLink PL-A662 (USA) microscope camera coupled to an Edmund Optics (UK) 63.745 objective (1.0X; working distance of 40 mm) and were analyzed using *OpenDrop* software [57]. As shown in Fig. 6.a, droplets on the surface of a bare ZTC electrode exhibit significant hydrophobicity. However, when carbon is coated with PDADMAC, as shown in Fig. 6.b, the contact angle decreases, indicating increased wettability. This

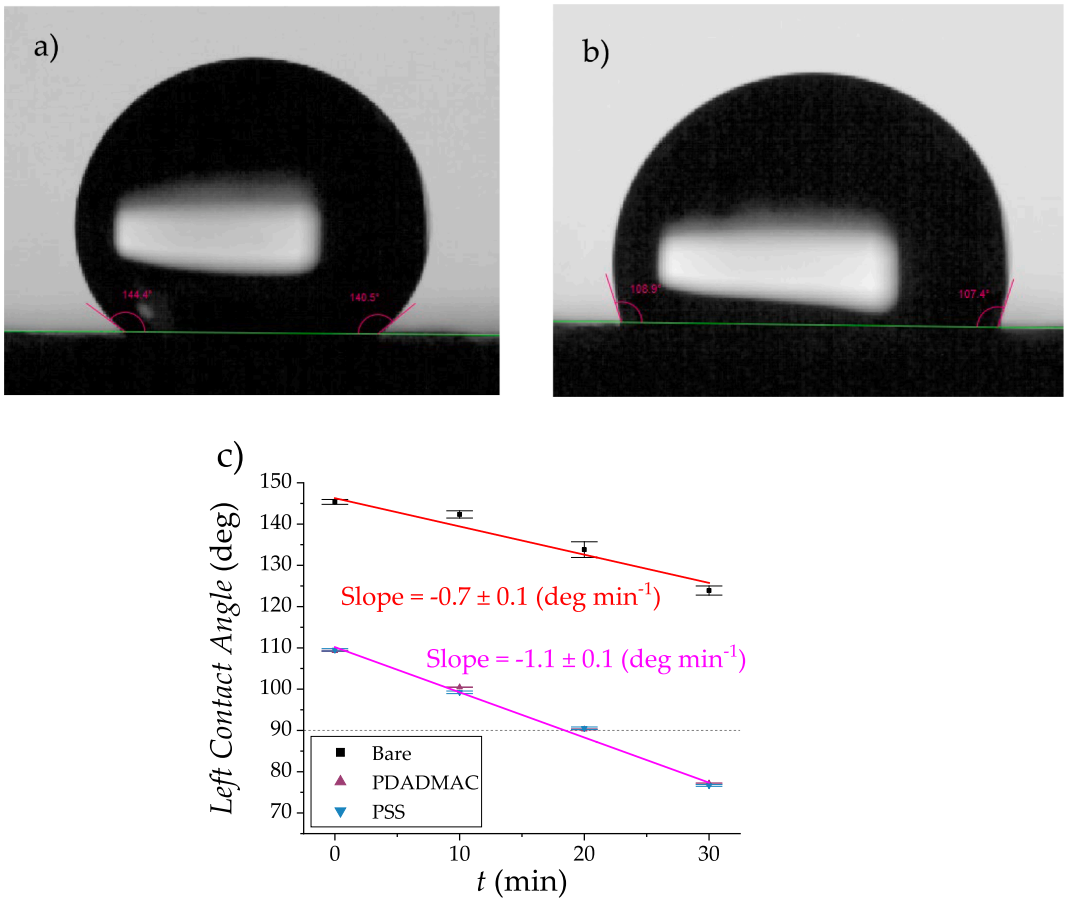

Fig. 6. Photographs of a water droplet on bare (a) and pdadmac-coated (b) ZTC substrates right after the water deposition; the measured contact angles are indicated. c) Contact angle of a water droplet as a function of time on a ZTC bare substrate (black), as well as on PDADMAC-(purple) and PSS- (blue) coated ones. Linear fittings are included for both systems. (For interpretation of the references to colour in this figure legend, the reader is referred to the web version of this article.)

behavior has also been observed with PSS-coated electrodes, confirming that polymer-covered ZTC exhibits higher wettability than bare ZTC, even immediately after contact with the liquid.

Although initial measurements show hydrophobic values for each of the evaluated systems, the contact angle for soft electrodes decreases at a slightly faster rate than bare electrodes and eventually reaches values lower than 90 degrees. Fig. 4.c shows the temporal changes observed over 30 min after droplet deposition. Overall, polymers enhance the wetting of the underlying zeolite-templated carbon material, leading to improved water flow through the material pores, and potentially more efficient desalination processes.

5.3. Energy extraction from salinity differences

5.3.1. Open circuit voltage

For each of the functionalized or membrane-assisted electrodes, Open Circuit Voltage differences (OCV) were measured as a function of time while a 500 mM KCl solution (which acts as salty solution) is exchanged with a solution 20 mM KCl, that is used as “fresh” solution. Recall that the observed voltage rise (in absolute value) when exchanging salinities is determinant for the energy and power obtained per cycle and would be a measure of the Donnan potential variations on both electrodes when the solutions are exchanged.

The maximum theoretical voltage rise for CDP using membranes is 145 mV, as reported in the literature [29]. For SEs, a numerical approximation has been made by solving the Poisson-Boltzmann equation and determining the electric potential inside the polyelectrolyte layer as described for the single-layered electrode setup [31,47,52]. The potential difference between the salty and fresh solution cases has been calculated using an ideal model and represented in Fig. 7.a as a function of the polymer charge density, ρ_{pol}. The greater the polymer charge, the larger the voltage rise will be, until it reaches a plateau that approaches the theoretical limit of 166 mV for this salt concentration difference.

Fig. 7b shows the experimental voltage rise for each of the systems in our experiments. In the case of membrane-assisted electrodes it reaches (114 ± 2) mV, while for SEs it is up to (71 ± 2) mV, showing the higher Donnan potential of the membranes over the polyelectrolyte coating, and thus its higher volumetric charge density. The combination of both SEs and IEMs gives way to a higher value for the voltage rise of about 131 mV.

The kinetics of each of the curves plays an important role, as not only the voltage rise will determine the performance of the system, but also the timescale of the measurement is crucial in the power generation, which will be higher for shorter cycle times. Therefore, we highlight the SEs + IEMs combination not only for the improvement in voltage rise over the use of SEs and membranes by themselves, but also for the timescale reduction of the process over SEs, which makes an even higher difference in power production, as will be seen below.

The observed kinetic differences in electrodes involving polyelectrolyte coatings compared to ion-exchange membranes can be explained. In the latter, a notable advantage arises from the fact that the membrane potential is established as soon as the exchanged solution baths the electrode, resulting in the rapid establishment of a concentration difference across the IEMs. Consequently, the formation of a Donnan potential is expedited, significantly enhancing the kinetics of electrochemical processes. Furthermore, this arrangement allows a

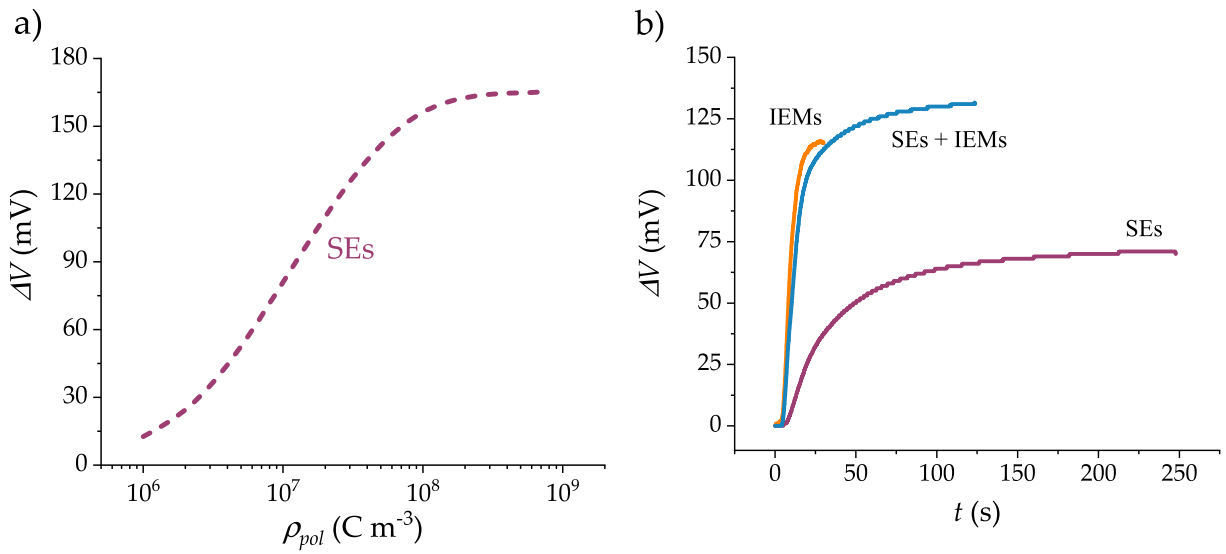

Fig. 7. a) Potential difference as a function of the polymer charge density calculated numerically. Solutions used for setting the different potentials were 500 mM and 20 mM KCl. b) Open Circuit Voltage difference measurements as a function of time for IEM-assisted electrodes (IEMs), soft electrodes (SEs) and soft-electrode/ion exchange membrane combination (SEs + IEMs) when exchanging salinities of the flowing solution.

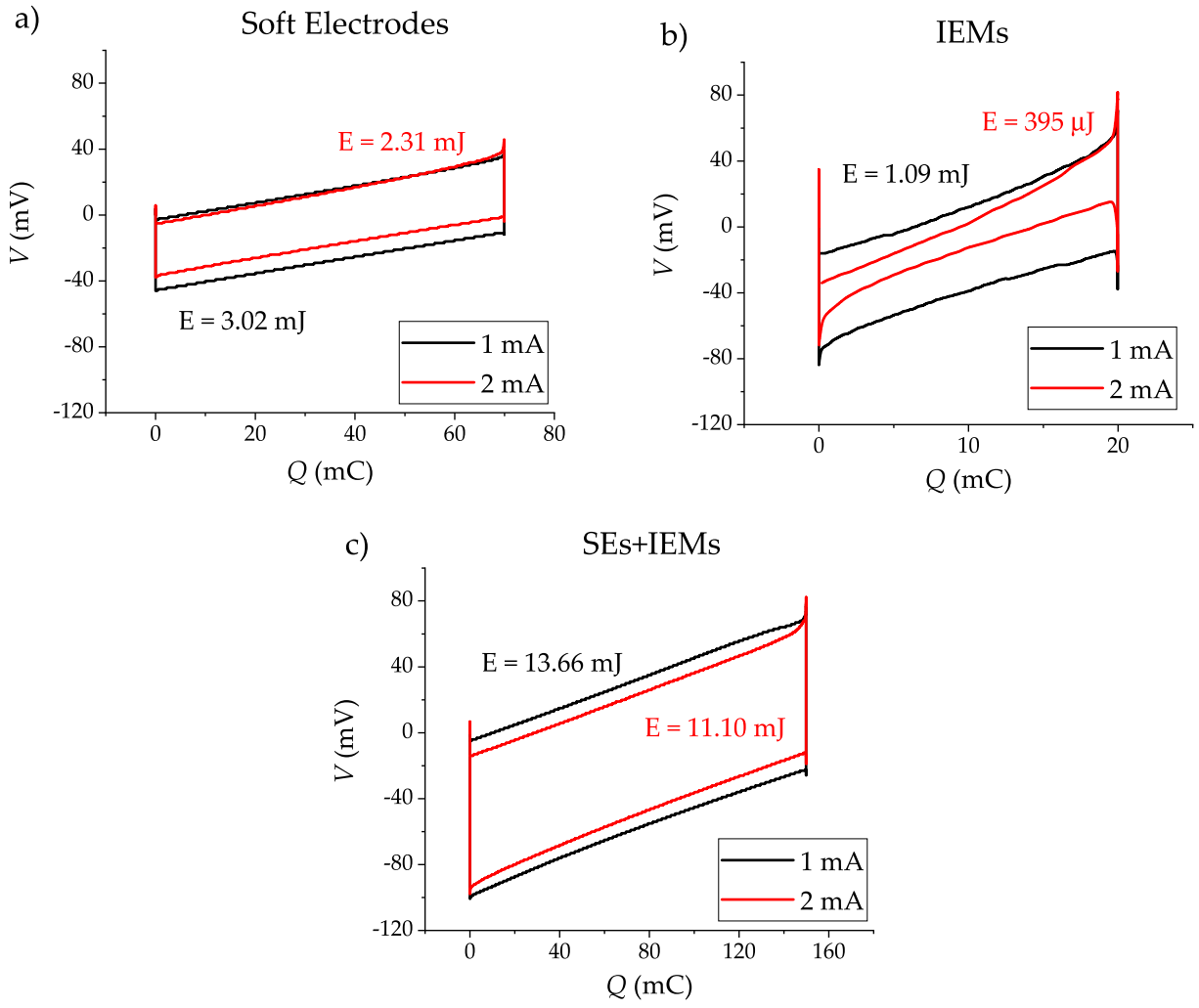

Fig. 8. Measured electric potential differences as function of the cell charge in a CapMix cycle using SEs (a), IEMs (b) and SEs + IEMs (c). Constant current values of ± 1 mA (black lines) and ± 2 mA (red lines) were applied during charge transfer steps. Transfer time values for 2 mA were half those used for 1 mA; open circuit stage duration when pumping salty and fresh solutions were equal for both currents. (For interpretation of the references to colour in this figure legend, the reader is referred to the web version of this article.)

rapid access of ions to the macropores, and subsequently to the micropores, thus promoting efficient ion transfer.

On the other hand, in the polyelectrolyte-coating case, it is important to note that the Donnan potential rise takes a longer time as compared to IEMs. The reason is that the coating penetrates the electrodes, lining the walls of macropores. When the salty electrolyte solution is exchanged for the fresh one, ions need to move through the porous electrode, reaching the micropores after a time given by diffusion, longer than the characteristic electromigration time. Consequently, the establishment of a concentration difference and the subsequent increase of the Donnan potential are delayed.

5.3.2. Method I (natural charge transfer)

In Fig. 8, individual electric potential vs. stored charge cycles have been represented for each electrode configuration and applied current when using Method I. A narrowing of the curves can be observed right after switching salinities in the step of charge transfer. This is more noticeable the higher the internal resistance (R_{int}) of the system and is magnified when the current applied upon closing the circuit is greater (under conditions of equal internal resistance) [29] since the observed potential drop is equal to IR_{int}. As fresh solutions are less conductive than salty ones, the ohmic potential drop is higher in the cycle stages where the electrodes are bathed by a fresh solution. It is also observed that the curves corresponding to constant currents of 2 mA have smaller enclosed areas, and therefore less energy obtained per cycle. However, the cycle execution time must be taken into account for the obtained power, since the use of higher currents for an equal total stored charge implies a shorter transfer time for it.

This phenomenon can be seen more distinctly in cases involving the use of membranes than in cases with SEs for both applied currents, and it is one of the reasons why more energy is obtained from those cycles even though the observed ΔV is lower. SEs appear to minimally impact the internal resistance of the system, which is also evidenced by the observation that placing membranes adjacent to SEs does not result in a substantial increase in electric potential leakages [6]. The polyelectrolyte coatings render the electrodes highly conductive, consequently counteracting larger potential leaks that would otherwise be caused by the membranes.

Tables 2 and 3 show the quantitative values of the open circuit voltage rise (ΔV) measured, and the obtained energy (E) and power (P) per cycle, respectively for 1 mA and 2 mA, when exchanging from a salty to a fresh solution after transferring charge, depending on the experimental parameters described above.

Exceptionally high values of energy per cycle were obtained when using SEs for the CapMix technique, reaching up to 3.01 mJ in the case where 1 mA was the applied current. Even though the energy is more than three times the highest value reported in a previous work [47], the obtained power values are still slightly lower than the 4.30 mW m^{-2} reported for the cases where both salty and fresh solutions were exchanged at a temperature of 25 °C.

The combination of SEs with IEMs marks an improvement in the overall achievements for the CapMix technique: values of 13.66 mJ per cycle and 7.43 mW m^{-2} were reached when applying constant currents of 1 mA, while 11.10 mJ per cycle and 10.09 mW m^{-2} were obtained for the 2 mA case, clearly overcoming the reference value mentioned above.

Table 3
Same as Table 2, but with 2 mA applied current.

Method I – 2 mA						
Electrode configuration	Charge transfer time (s)	Open Circuit Salty// Fresh times (s)	ΔV_{OCV} (mV)	ΔV (mV)	E (mJ)	P (mW m^{-2})
SEs	35	40//70	71 ± 1	48 ± 1	2.31 ± 0.01	2.63 ± 0.01
IEMs	10	20//20	114 ± 1	67 ± 1	0.39 ± 0.01	1.02 ± 0.01
SEs + IEMs	75	30//40	131 ± 1	95 ± 1	11.10 ± 0.01	10.09 ± 0.01

5.3.3. Method II (extended charge transfer)

As mentioned, charge transfer times were doubled for this method, which results in the horizontal expansion of the curves. Fig. 9 shows individual electric potential vs. stored charge cycles, represented for each electrode configuration, comparing both Method I and Method II when applying 1 mA. As the charge window doubles for Method II, the curves suffer a noticeable narrowing that will be relevant for the energy gain, as potential decreases and responds in a non-linear way to charging and discharging. Thus, the potential leakage increases and becomes not negligible as the total stored charge in the system increases. According to the literature [29], this is due to the non-ideal behaviour of the membranes, as well as the self-discharge of the capacitive system, which would be the cause of the non-linear relationship between the electric potential and accumulated charge. Table 4 shows the quantitative values obtained from the measurements made following Method II. In general, the same behaviour is observed depending on the type of electrode: SEs and their combination with membranes provide the best results in terms of energy and power.

When comparing Methods I and II, a slight increase in the energy obtained is observed in the extended method when using SEs and IEMs separately despite the narrowing of the curve in the steps corresponding to electric charge transfer. Due to the minor difference in energy and the increase in cycle duration, more power is still obtained in the non-extended method. The clear exception is the SEs + IEMs combination, where in addition to a huge difference in energy (almost double than obtained in Method I), there is also a slight improvement in power when Method II is used. This setup avoids the leakage that tightens the area of the cycle. This allows the production of much higher energy than in non-extended cases, without sacrificing power in the process.

6. Conclusions

Polyelectrolyte coating onto zeolite-templated carbon (ZTC), a highly porous material with ordered pore distribution, has demonstrated to be a suitable combination for energy harvesting and water purification applications. When tested for capacitive deionization (CDI), soft ZTC electrodes (carbon/polyelectrolyte or SEs) yield high amounts of salt withdrawn from the contacting solution, with relatively low energy cost ($20k_BT$ per ion removed). Even at high salt concentrations (100 mM NaCl), the system has a notorious SAC (specific adsorption

Table 2
Measured Open Circuit Voltage (ΔV_{OCV}) and voltage rise during cycles (ΔV) upon exchanging salinities of the bathing solution, and obtained energy per cycle (E) and specific power (P) when following Method I with 1 mA applied current.

Method I – 1 mA						
Electrodeconfiguration	Charge transfer time (s)	Open Circuit Salty//Fresh times (s)	ΔV_{OCV} (mV)	ΔV (mV)	E (mJ)	P (mW m^{-2})
SEs	70	40//70	71 ± 1	50 ± 1	3.01 ± 0.01	2.41 ± 0.01
IEMs	20	20//20	114 ± 1	86 ± 1	1.09 ± 0.01	2.61 ± 0.01
SEs + IEMs	150	30//40	131 ± 1	100 ± 1	13.66 ± 0.01	7.43 ± 0.01

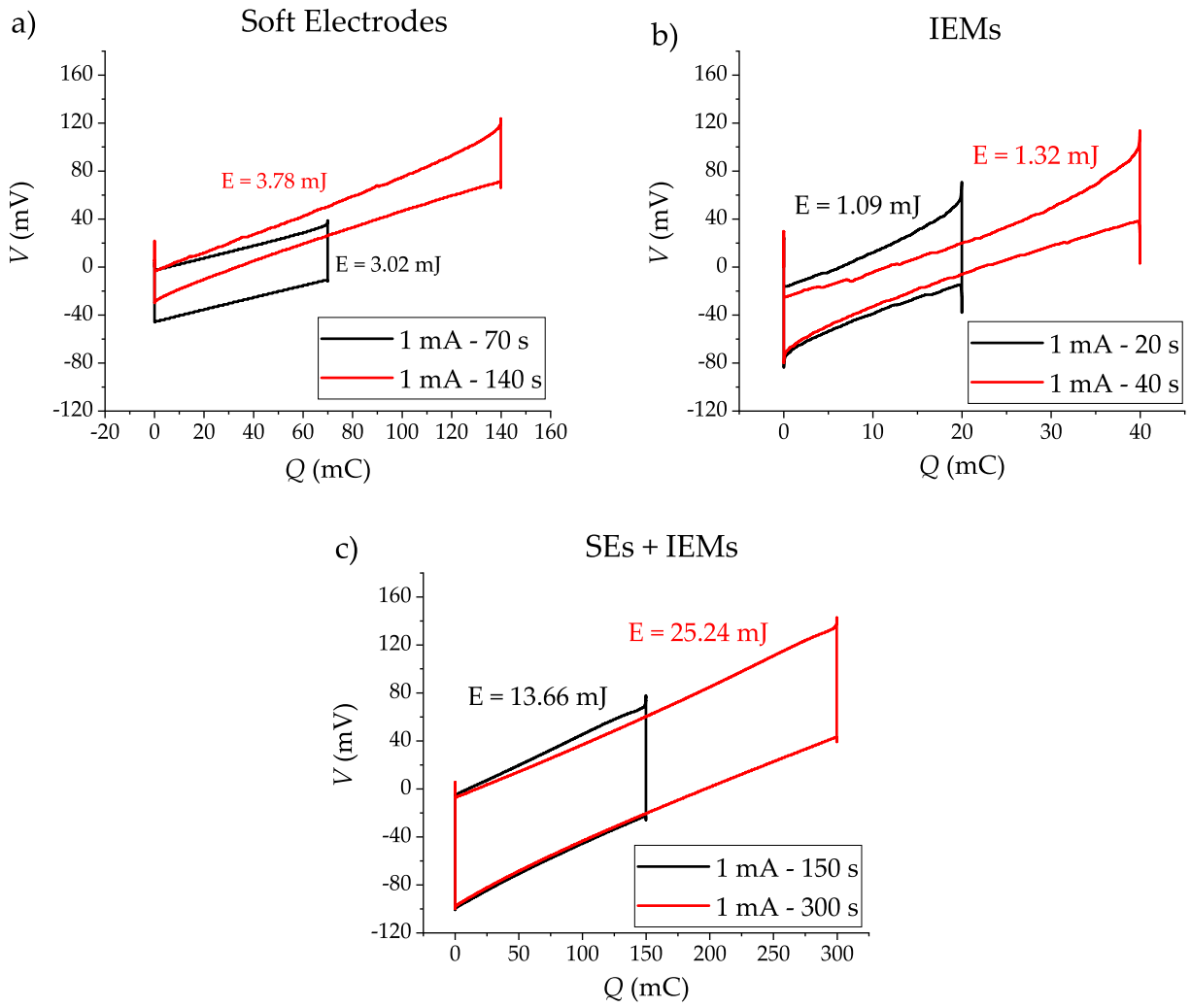

Fig. 9. Measured electric potential differences as function of the cell charge in a CapMix cycle using SEs (a), IEMs (b) and SEs + IEMs (c). Black curves correspond to Method I measurements, and red curves correspond to Method II. Constant current values of ± 1 mA were set for charge transfer steps. Open circuit times when pumping salty and fresh solutions were equal for both methods.

Table 4
Measured Open Circuit Voltage (ΔV_{OCV}) and voltage rise during cycles (ΔV) upon exchanging salinities of the bathing solution, and obtained energy per cycle (E) and power (P) when following Method II with 1 mA as applied current.

Method II – 1 mA – Extended charge						
Electrode configuration	Charge transfer time (s)	Open Circuit Salty// Fresh times (s)	ΔV_{OCV} (mV)	ΔV (mV)	E (mJ)	P (mW m^{-2})
SEs	140	40//70	71 ± 1	53 ± 1	3.78 ± 0.01	2.21 ± 0.01
IEMs	40	20//20	114 ± 1	76 ± 1	1.32 ± 0.01	2.08 ± 0.01
SEs + IEMs	300	30//40	131 ± 1	100 ± 1	25.24 ± 0.01	7.50 ± 0.01

capacity) of 25.3 mg/g with efficiency close to unity. This is very promising for high-salinity water desalination [16,55], where CDI not always performs satisfactorily.

In this work it has been demonstrated, for the first time, how soft ZTC electrodes are able to generate energy by salinity differences. The results obtained with the combination of SEs and ion exchange membranes (IEMs) show an improvement over the overall performance of each technique separately. SEs act as a good support for the membranes and allow harvesting significant amounts of energy by taking benefit of the potential rise obtained with IEMs, but minimizing the leakages associated to them. Electric potential drops associated to the internal resistance of the system decreased when polyelectrolytes were present, and non-linearities observed in the potential-charge relationships were minimized when using higher currents for charging/discharging, which allowed a reduction in cycle time, resulting in higher power per area. In addition, it has been investigated the extension of the charge transfer windows by applying current beyond the condition of zero potential difference between electrodes (Method II), without important potential leakages, reaching outstanding values of energy per cycle (up to 25.24 mJ) and power, which resulted to be larger than the ones obtained when applying the same current values up to equipotentiality (Method I).

The choice of electrode material, such as zeolite-tailored carbon, and the use of strategies like polyelectrolyte coating and IEM supports produce evident advances in efficiency, reliability, and sustainability of CDI and CapMix technologies, taking the surface properties of the carbon material one step further.

Funding Sources

Financial support of this investigation by the grant TED2021-131855BI00/AEI/https://doi.org/10.13039/501100011033/Unión

Europea Next Generation EU/PRTR is gratefully acknowledged. Funding for open access charge: Universidad de Granada / CBUA.

CRediT authorship contribution statement

Sergio Orozco-Barrera: Software, Investigation, Data curation. **Keigo Wakabayashi:** Data curation, Investigation. **Takeharu Yoshii:** Methodology, Investigation, Writing – review & editing. **Hirotomo Nishihara:** Supervision, Methodology, Writing – review & editing. **Guillermo R. Iglesias:** Methodology, Writing – review & editing. **Ángel V. Delgado:** Supervision, Methodology, Writing – review & editing. **Silvia Ahualli:** Validation, Conceptualization, Visualization.

Declaration of competing interest

The authors declare that they have no known competing financial interests or personal relationships that could have appeared to influence the work reported in this paper.

Data availability

Data will be made available on request.

Appendix A. Supplementary data

Additional adsorption and SAC figures and tables corresponding to ZTC SE+IEMs electrode configuration working with different operational voltages (Figure S1 and Table S1) and when desalinating a higher concentration solution (Figure S2 and Table S2) (DOC). Supplementary data to this article can be found online at https://doi.org/10.1016/j.seppur.2024.129314.

References

[1] A.V. Delgado, M.L. Jimenez, G.R. Iglesias, S. Ahualli, Electrical double layers as ion reservoirs: applications to the deionization of solutions, Curr. Opin. Colloid Interface Sci. 44 (2019) 72–84.
[2] Á.V. Delgado, Interfacial electrokinetics and electrophoresis, CRC Press 106 (2001).
[3] M.M. AL-Rajabi, F.A. Abumadi, T. Laoui, M.A. Atieh, K.A. Khalil, Capacitive deionization for water desalination: Cost analysis, recent advances, and process optimization, J. Water Process Eng. 58 (2024) 104816.
[4] S.D. Datar, R. Mane, N. Jha, Recent progress in materials and architectures for capacitive deionization: A comprehensive review, Water Environ. Res 94 (2022) e10696.
[5] N.Y. Yip, D. Brogioli, H.V.M. Hamelers, K. Nijmeijer, Salinity gradients for sustainable energy: primer, progress, and prospects, Environ. Sci. Tech. 50 (2016) 12072–12094.
[6] M.M. Fernandez, R.M. Wagterveld, S. Ahualli, F. Liu, A.V. Delgado, H.V. M. Hamelers, Polyelectrolyte-versus membrane-coated electrodes for energy production by capmix salinity exchange methods, J. Power Sources 302 (2016) 387–393.
[7] D. Brogioli, Extracting renewable energy from a salinity difference using a capacitor, Phys. Rev. Lett. 103 (2009).
[8] D. Brogioli, R. Zhao, P.M. Biesheuvel, A prototype cell for extracting energy from a water salinity difference by means of double layer expansion in nanoporous carbon electrodes, Energ. Environ. Sci. 4 (2011) 772–777.
[9] S. Ahualli, A.V. Delgado, Charge and Energy Storage in Electrical Double Layers, Academic Press, 2018.
[10] S. Porada, R. Zhao, A. van der Wal, V. Presser, P.M. Biesheuvel, Review on the science and technology of water desalination by capacitive deionization, Prog. Mater Sci. 58 (2013) 1388–1442.
[11] B.P. Jia, L.D. Zou, Graphene nanosheets reduced by a multi-step process as high-performance electrode material for capacitive deionisation, Carbon 50 (2012) 2315–2321.
[12] G. Rasines, P. Lavela, C. Macias, M.C. Zafra, J.L. Tirado, J.B. Parra, C.O. Ania, N-doped monolithic carbon aerogel electrodes with optimized features for the electrosorption of ions, Carbon 83 (2015) 262–274.
[13] J. Ma, L. Wang, F. Yu, Water-enhanced performance in capacitive deionization for desalination based on graphene gel as electrode material, Electrochim. Acta 263 (2018) 40–46.
[14] Y. Zhang, P. Ren, Y. Liu, V. Presser, Particle size distribution influence on capacitive deionization: Insights for electrode preparation, Desalination 525 (2022) 115503.
[15] X. Zhao, H. Wei, H. Zhao, Y. Wang, N. Tang, Electrode materials for capacitive deionization: A review, J. Electroanal. Chem. 873 (2020) 114416.
[16] P. Zhang, J. Li, M.B. Chan-Park, Hierarchical porous carbon for high-performance capacitive desalination of brackish water, ACS Sustain. Chem. Eng. 8 (2020) 9291–9300.
[17] Y. Liu, X. Xu, M. Wang, T. Lu, Z. Sun, L. Pan, Metal–organic framework-derived porous carbon polyhedra for highly efficient capacitive deionization, Chem. Commun. 51 (2015) 12020–12023.
[18] H. Nishihara, T. Kyotani, Zeolite-Templated Carbon - Its Unique Characteristics and Applications, Novel Carbon Adsorbents (2012) 295–322.
[19] H. Nishihara, T. Kyotani, Zeolite-templated carbons - three-dimensional microporous graphene frameworks, Chem. Commun. 54 (2018) 5648–5673.
[20] J.M. Rosas, R. Ruiz-Rosas, R. Berenguer, D. Cazorla-Amoros, E. Morallon, H. Nishihara, T. Kyotani, J. Rodriguez-Mirasol, T. Cordero, Easy fabrication of superporous zeolite templated carbon electrodes by electrospraying on rigid and flexible substrates, J. Mater. Chem. A 4 (2016) 4610–4618.
[21] H. Nishihara, T. Kyotani, Templated Nanocarbons for Energy Storage, Adv. Mater. 24 (2012) 4473–4498.
[22] H. Nishihara, K. Imai, H. Itoi, K. Nomura, K. Takai, T. Kyotani, Formation Mechanism of Zeolite-Templated Carbons, Carbon 175 (2021) 605.
[23] H. Itoi, H. Nishihara, T. Kogure, T. Kyotani, Three-dimensionally arrayed and mutually connected 1.2-nm nanopores for high-performance electric double layer capacitor, J. Am. Chem. Soc. 133 (2011) 1165–1167.
[24] P.M. Biesheuvel, A. van der Wal, Membrane capacitive deionization, J. Membr. Sci. 346 (2010) 256–262.
[25] J.Y. Lee, S.J. Seo, S.H. Yun, S.H. Moon, Preparation of ion exchanger layered electrodes for advanced membrane capacitive deionization (MCDI), Water Res. 45 (2011) 5375–5380.
[26] A. Hassanvand, K.J. Wei, S. Talebi, G.Q. Chen, S.E. Kentish, The role of ion exchange membranes in membrane capacitive deionisation, Membranes 7 (2017).
[27] H.B. Li, L. Zou, Ion-exchange membrane capacitive deionization: A new strategy for brackish water desalination, Desalination 275 (2011) 62–66.
[28] R. McNair, G. Szekely, R.A. Dryfe, Ion-exchange materials for membrane capacitive deionization, ACS Environ. Sci. Technol. Water 1 (2020) 217–239.
[29] F. Liu, O. Schaetzle, B.B. Sales, M. Saakes, C.J.N. Buisman, H.V.M. Hamelers, Effect of additional charging and current density on the performance of Capacitive energy extraction based on Donnan Potential, Energ. Environ. Sci. 5 (2012) 8642–8650.
[30] S. Ahualli, M.M. Fernández, Á.V. Delgado, G.R. Iglesias, CDP: Fundamentals of the Method, in: In Interface Science and Technology, Elsevier, 2018, pp. 143–166.
[31] S. Ahualli, G.R. Iglesias, M.M. Fernandez, M.L. Jimenez, A.V. Delgado, Use of soft electrodes in capacitive deionization of solutions, Environ. Sci. Tech. 51 (2017) 5326–5333.
[32] Y.J. Kim, J.H. Choi, Improvement of desalination efficiency in capacitive deionization using a carbon electrode coated with an ion-exchange polymer, Water Res. 44 (2010) 990–996.
[33] K. Jo, Y. Baek, S. Kim, S.P. Hong, J. Yoon, Evaluation of long-term stability in capacitive deionization using activated carbon electrodes coated with ion exchange polymers, Korean J. Chem. Eng. 37 (2020) 1199–1205.
[34] S. Ahualli, M.L. Jimenez, M.M. Fernandez, G. Iglesias, D. Brogioli, A.V. Delgado, Polyelectrolyte-coated carbons used in the generation of blue energy from salinity differences, PCCP 16 (2014) 25241–25246.
[35] S. Ahualli, S. Orozco-Barrera, M.d.M. Fernández, Á.V. Delgado, G.R. Iglesias, Assembly of soft electrodes and ion exchange membranes for capacitive deionization, Polymers 11 (2019) 1556.
[36] G.R. Iglesias, S. Ahualli, A.V. Delgado, P.M. Arenas-Fernandez, M.M. Fernandez, Combining soft electrode and ion exchange membranes for increasing salinity difference energy efficiency, J. Power Sources 453 (2020) 227840.
[37] J. Miao, Z. Lang, T. Xue, Y. Li, Y. Li, J. Cheng, H. Zhang, Z. Tang, Revival of zeolite-templated nanocarbon materials: recent advances in energy storage and conversion, Adv. Sci. 7 (2020) 2001335.
[38] S. Khan, H. Park, K. Kim, H. Park, R. Ryoo, Hierarchically porous zeolite-templated carbon embedded with manganese oxide for long-cycling asymmetric supercapacitor, Microporous Mesoporous Mater. (2024), 113050.
[39] H.C. Kwon, S. Choi, Y. Wang, R. Othman, M. Choi, Scalable synthesis of zeolite-templated ordered microporous carbons without external carbon deposition for capacitive energy storage, Microporous Mesoporous Mater. 307 (2020), 110481.
[40] M. Ren, C.-Y. Zhang, Y.-L. Wang, J.-J. Cai, Development of N-doped carbons from zeolite-templating route as potential electrode materials for symmetric supercapacitors, Int. J. Miner. Metall. Mater. 25 (2018) 1482–1492.
[41] K. Nueangnoraj, IEEE. Zeolite-Templated Carbon as Electrodes for Electrochemical Energy Storage, in: 2016 Second Asian Conference on Defence Technology (acdt), 2016, pp. 179–182.
[42] K. Li, S. Zhu, S. Zhao, M. Gong, X. Zhao, J. Liang, J. Gan, Y. Huang, M. Zhao, D. Zhuang, Synthesis of nitrogen-doped carbon nanoboxes with pore structure derived from zeolite and their excellent performance in capacitive deionization, J. Mater. Chem. A 12 (2024) 899–910.
[43] M.E. Suss, S. Porada, X. Sun, P.M. Biesheuvel, J. Yoon, V. Presser, Water desalination via capacitive deionization: what is it and what can we expect from it? Energ. Environ. Sci. 8 (2015) 2296–2319.
[44] S. Porada, L. Borchardt, M. Oschatz, M. Bryjak, J.S. Atchison, K.J. Keesman, S. Kaskel, P.M. Biesheuvel, V. Presser, Direct prediction of the desalination performance of porous carbon electrodes for capacitive deionization, Energ. Environ. Sci. 6 (2013) 3700–3712.
[45] S. Ahualli, G.R. Iglesias, Á.V. Delgado, Principles and theoretical models of CDI: Experimental approaches, in: Interface Science and Technology, Elsevier, 2018, pp. 169–192.
[46] R. Zhao, P.M. Biesheuvel, H. Miedema, H. Bruning, A. van der Wal, Charge efficiency: a functional tool to probe the double-layer structure inside of porous

electrodes and application in the modeling of capacitive deionization, J. Phys. Chem. Lett. 1 (2010) 205–210.
[47] S. Ahualli, M.L. Jimenez, Z. Amador, M.M. Fernandez, G.R. Iglesias, A.V. Delgado, Energy production by salinity exchange in polyelectrolyte-coated electrodes. Temperature Effects, Sustain. Energy Fuels 5 (2021) 3321–3329.
[48] S. Nadakatti, M. Tendulkar, M. Kadam, Use of mesoporous conductive carbon black to enhance performance of activated carbon electrodes in capacitive deionization technology, Desalination 268 (2011) 182–188.
[49] K. Kaneko, C. Ishii, Superhigh surface area determination of microporous solids, Colloids Surf. 67 (C) (1992) 203–212.
[50] Z. Ryu, J. Zheng, M. Wang, B. Zhang, Characterization of pore size distributions on carbonaceous adsorbents by DFT, Carbon 37 (8) (1999) 1257–1264.
[51] H. Nishihara, Q.H. Yang, P.H. Hou, M. Unno, S. Yamauchi, R. Saito, J.I. Paredes, A. Martínez-Alonso, J.M.D. Tascón, Y. Sato, M. Terauchi, T. Kyotani, A possible buckybowl-like structure of zeolite templated carbon, Carbon 47 (2009) 1220–1230.
[52] S. Orozco-Barrera, G.R. Iglesias, A.V. Delgado, S. Garcia-Larios, S. Ahualli, Effects of layer-by-layer coating on activated carbon electrodes for capacitive deionization, PCCP 25 (2023) 9482–9491.
[53] M. Torkamanzadeh, C. Kök, P.R. Burger, P. Ren, Y. Zhang, J. Lee, C. Kim, V. Presser, Best practice for electrochemical water desalination data generation and analysis, Cell Rep. Phys. Sci. 4 (2023) 101661.
[54] L. Wang, Y. Zhang, K. Moh, V. Presser, From capacitive deionization to desalination batteries and desalination fuel cells, Curr. Opin. Electrochem. 29 (2021) 100758.
[55] Y. Zhang, C. Prehal, H. Jiang, Y. Liu, G. Feng, V. Presser, Ionophobicity of carbon sub-nanometer pores enables efficient desalination at high salinity, Cell Rep. Phys. Sci. 3 (1) (2022) 100689.
[56] S. Bi, Y. Zhang, L. Cervini, T. Mo, J.M. Griffin, V. Presser, G. Feng, Permselective ion electrosorption of subnanometer pores at high molar strength enables capacitive deionization of saline water, Sustain. Energy Fuels 4 (2020) 1285–1295.
[57] E. Huang, A. Skoufis, T. Denning, J. Qi, R.R. Dagastine, R.F. Tabor, J.D. Berry, OpenDrop: Open-source software for pendant drop tensiometry & contact angle measurements, J. Open Source Software 6 (2021) 2604.